Published in final edited form as:
J Biomater Sci Polym Ed. 2013 September ; 24(13): 1529–1548. doi:10.1080/09205063.2013.777228.

Hemocompatibility of Polymeric Nanostructured Surfaces

Victoria Leszczak[1], **Barbara S. Smith**[2], and **Ketul C. Popat**[1,2,*]

[1]Department of Mechanical Engineering, Colorado State University, Fort Collins, CO 80523

[2]School of Biomedical Engineering, Colorado State University, Fort Collins, CO 80523

Abstract

Tissue integration is an important property when inducing transplant tolerance, however, the hemocompatibility of the biomaterial surface also plays an important role in the ultimate success of the implant. Therefore, in order to induce transplant tolerance, it is critical to understand the interaction of blood components with the material surfaces. In this study, we have investigated the adsorption of key blood serum proteins, in vitro adhesion and activation of platelets and clotting kinetics of whole blood on flat polycaprolactone (PCL) surfaces, nanowire (NW) surfaces and nanofiber (NF) surfaces. Previous studies have shown that polymeric nanostructured surfaces improve cell adhesion, proliferation and viability; however it is unclear how these polymeric nanostructured surfaces interact with the blood and its components. Protein adsorption results indicate that while there were no significant differences in total albumin adsorption on PCL, NW and NF surfaces, NW surfaces had higher total fibrinogen and immunoglobulin-G adsorption compared to NF and PCL surfaces. In contrast, NF surfaces had higher surface FIB and IgG adsorption compared to PCL and NW surfaces. Platelet adhesion and viability studies show more adhesion and clustering of platelets on the NF surfaces as compared to PCL and NW surfaces. Platelet activation studies reveal that NW surfaces have the highest percentage of unactivated platelets, whereas NF surfaces have the highest percentage of fully activated platelets. Whole blood clotting results indicate that NW surfaces maintain an increased amount of free hemoglobin during the clotting process compared to PCL and NF surface, indicating less clotting and slower rate of clotting on their surfaces.

Keywords

Hemocompatibility; nanowire surfaces; nanofiber surfaces; platelets

1. INTRODUCTION

Cardiovascular disease is the leading cause of death worldwide killing 17.3 million people a year [1]. Current treatments for cardiovascular diseases include organ transplants, surgery, metabolic products and mechanical/synthetic implants [2]. Of these, mechanical and synthetic implants have shown great promise in recent years. Metals, natural polymers and synthetic polymers have been used in these mechanical and synthetic cardiovascular implants [3, 4]. However, synthetic polymers have been recognized as better candidates for cardiovascular repair due to the thrombogenic nature of metals and limit in processability of natural polymers [5, 6]. In particular, synthetic polymers such as polyurethane [7], poly(L-lactic acid) [8], polyglycolic acid [9] and polycaprolactone [10] have proven to be of tremendous use due to their biocompatibility and controlled mechanical properties. These polymers have been used to develop cardiovascular devices such as vascular grafts [11],

*Author of correspondence: Ketul.Popat@ColoState.EDU.

artificial hearts [12], and heart valves [13], all of which have been widely used in recent years [14]. These implants have the potential to replace the damaged components of the cardiovascular system, while maintaining the normal tissue function. Tissue integration is important property when inducing transplant tolerance, however, the hemocompatibility of the biomaterial surface also plays an important role in the ultimate success of the implant. Therefore, in order to induce transplant tolerance, it is critical to understand the interaction of blood components with the material surfaces [15, 16]. Hemocompatibility is an essential property of biomaterials and can be measured by the interaction between the material and the various blood components, such as blood plasma proteins, erythrocytes, platelets and leukocytes [17]. Lack of hemocompatibility can lead to either rejection and/or loss of function [18] initially through the activation of the blood coagulation cascade followed by initiation of immune responses [19]. Blood reactions occur as a result of the physical and chemical properties of implant surface, therefore tolerance can potentially be achieved by altering the biomaterial surface properties [20].

When a biomaterial is implanted inside the body, proteins are adsorbed on the material surface [21], followed by platelet adhesion and activation, eventually leading to the formation of thrombus [22]. Previous work has investigated various surface modifications strategies to alter the hemocompatibility of biomaterial surfaces [23–25]. Inorganic and organic coatings [26], polymer surface chemical modification [27], and chemically patterned surfaces [28] have been used to alter hemocompatibility. These surfaces have proven to produce favorable hemocompatible response through inertness, chemical and mechanical stability, and low protein adsorption [19, 28]. Unfortunately, these surfaces are not stable when exposed to the shear stresses of blood flow [29], thus it is important to have a robust surface that can withstand physiological forces. The hierarchy of the natural tissue extracellular matrix (ECM), from nano to macro scale, has inspired fabrication of surfaces with different topographies. In recent years, nanostructured surfaces have emerged as a potential solution to improve material integration with the tissue. Studies have shown that surfaces that mimic the ECM nanotopography can promote tissue integration and regeneration [30]. Thus, polymers with tunable properties have been extensively researched. Polymeric nanostructured surfaces have shown to affect cellular growth and functionality [31–33]. In particular, these surfaces have demonstrated improved fibroblast cell adhesion [34], neuronal cell differentiation [35], and osteoblast phenotypic activity [19, 36]. However, it is unclear how these polymeric nanostructured surfaces interact with the blood and its components. An understanding of blood/nanomaterial interaction is essential to understand how transplant tolerance is induced using nanostructured surfaces.

In this study, we have investigated the hemocompatibility of two different nanostructured surfaces: nanowires and nanofibers. These two nano-topographies were chosen because they have similar sized features that are aligned differently; nanowires are aligned perpendicular to the surface while nanofibers are aligned parallel to the surface. It is hypothesized that this alteration in the alignment of nanostructures on the surface will result in a very different response to blood components, thus altering the hemocompatibility. Polycaprolactone (PCL) was chosen as the material since it is a bioresorbable polyester with exceptional mechanical strength and low degradation rate [37]. PCL scaffolds have been used extensively in many tissue engineering applications, specifically for vascular tissue [38, 39], bone and cartilage [40, 41], nerve [42, 43], dental [44] and skin [45]. The low degradation rate of PCL is favorable for long-term implants [46, 47]. Further, degradation products of PCL in the body can be removed naturally by the metabolic pathways [3, 37, 48] eliminating the possibility of foreign body reactions. PCL can also be processed into unique nanostructured surfaces such as nanowires [49], thin film nanowires [50], nano-fibrous networks [51] and nanofibers [52–54]. These nanostructured features are capable of being tuned. For example, electrospinning has shown promising results with its ability to fabricate surfaces that mimic

the ECM hierarchy. By changing electrospinning parameters such as voltage, working distance and polymer concentration, the surface properties can be easily tuned to match the natural ECM hierarchy [55].

To evaluate interactions at the blood-nanomaterial interface, it is necessary to understand the events that occur during the introduction of a foreign object inside the body. Driven by a need for understanding potential biomedical and clinical uses of PCL nanostructured surfaces, this work specifically looks at the earliest stages of blood-material interaction by considering the in vitro adsorption of key blood serum proteins, adhesion and activation of platelets and clotting kinetics of whole blood. In this study blood serum protein adsorption on nanostructured surfaces was investigated using a colorimetric assay and X-ray photoelectron spectroscopy (XPS). Fluorescence microscopy and scanning electron microscope (SEM) were used to determine the adhesion and activation of platelets. A simple hemolysis assay was used to investigate the whole blood clotting kinetics. It was found surfaces fabricated from the same material (PCL) with altered nanotopography orientation, induce different hemocompatible response.

2. MATERIALS AND METHODS

2.1 Fabrication of PCL nanowire and nanofiber surfaces

Smooth PCL (control) surfaces (notation: PCL) were fabricated by sintering PCL pellets (MW = 80000, Sigma) on a glass plate in a 10mm Teflon washer. The resulting discs were then allowed to air-cool before being removed from the glass surface.

PCL nanowire surfaces (notation: NW) were fabricated utilizing the solvent free nanotemplating technique with commercially available 20nm diameter nanoporous aluminum oxide membranes (ANOPORE™, Whatman) [56]. Smooth PCL surfaces (as fabricated above) were placed on the membrane surface and placed in an oven at 115°C for 3–5mins, allowing the polymer to gravimetrically extrude through the membrane. The aluminum oxide membranes were dissolved in 1M NaOH for 75mins in order to release the extruded nanowires. The nanowire surfaces were then washed three times in DI water, dried and stored in a desiccator until further use.

PCL nanofiber (notation: NF) surfaces were fabricated by an electrospinning technique. The electrospinning apparatus consisted of a syringe pump, a glass syringe, teflon fluidic tubing, a 20-gauge blunt-tip catheter, and a male luer lock adapter. A high-voltage power source was connected to the catheter tip with a standard alligator clamp. The collector consisted of an aluminum foil fastened onto a 0.5″ thick copper plate with electrical tape and positioned horizontally below the catheter. Polymer solution was prepared by dissolving oleic acid sodium salt (OLA) in methanol. PCL pellets (MW = 80000) were dissolved in chloroform and the polymer solution was mixed with OLA in methanol on a magnetic stir plate to produce a homogeneous mixture with a 4:1 chloroform:methanol volume ratio. The final solution was 12% solid w/w and the PCL:OLA ratio of the solid weight was 97:3 [57]. The volumetric flow rate was 10ml/hr, applied voltage was 20 kV, and tip-to-collector was distance 9cm. Finally, OLA was leached out by placing nanostructured surfaces in methanol for 1h.

All the surfaces that were used for biological studies were approximately 1cm in diameter. The surfaces were sterilized in 70% ethanol for 30mins, followed by washing (2×) with PBS. They were air dried and further sterilized by uv exposure for 30mins before using for biological studies.

2.2 Characterization of PCL nanowire and nanofiber surfaces

The surface architecture of the nanostructured surfaces was characterized using scanning electron microscope (SEM, JEOL JSM-6300). The surfaces were coated with a 10nm layer of gold and imaged at 5–7kV. Nanowire and nanofiber diameters and heights were computed using the image analysis system built into the SEM.

Surface hydrophilicity was characterized by measuring the contact angle of DI water. A droplet of DI water, approximately 100 μL in volume, was formed on the tip of the syringe and the machine stage was moved upward so that the droplet contacted and detached onto the surface. The water droplet image on the surface was captured within 5secs after the contact by a camera leveled with the surface. Images were then analyzed with the accompanying software to measure the contact angles. Each experiment was performed on three different locations on each surface, and on at least three different surfaces (nmin = 9) [58].

2.3 Protein adsorption on PCL nanowire and nanofiber surfaces

In order to understand how key blood serum proteins interact with the nanostructured surfaces; albumin (ALB), fibrinogen (FIB) and immunoglobulin-G (IgG) (Sigma) adsorption was investigated on PCL, NW and NF surfaces. Sterilized surfaces were incubated in a 24-well plate with 100μg/ml solution of ALB, FIB and IgG in PBS on a horizontal shaker plate (100rpm) at 37oC and 5% CO_2. After 2hrs of incubation, the protein solution was aspirated followed by 3 rinses with PBS to remove any non-adherent proteins. The protein adsorption was measured using a commercially available micro-BCA assay (Pierce Biotechnology) and the adsorbed protein on nanostructured surfaces was visualized by SEM imaging.

In order to measure the protein adsorption using micro-BCA assay, all the surfaces were transferred to a fresh 24-well plate and incubated with 1% sodium dodecyl sulfate solution (SDS, Sigma) in PBS on a horizontal shaker plate (100rpm) for 1hr. Following incubation, the excess SDS solution with solubilized proteins was collected from each well. The SDS incubation was repeated 2 more times and the resulting SDS solution with solubilized proteins was pooled. The concentration of the total adsorbed protein in the pooled SDS solution was then measured colorimetrically using a micro-BCA assay with a plate reader.

X-ray photoelectron spectroscopy (XPS, ESCASystems X-ray Photoelectron Spectrometer 5800) was used to determine the surface composition of adsorbed proteins on nanostructured surfaces. High-resolution spectra were collected for C1s peak with a pass energy of 10eV. Peak fit analysis was performed using Multipack and XPSPeak 4.1 (Freeware) software.

Further, the protein adsorbed nanostructured surfaces were air dried and coated with a 10nm layer of gold and imaged at 5–7kV.

2.4 Platelet isolation from whole blood

Whole blood from healthy individuals, acquired through venopuncture, was drawn into standard 6ml vacuum tubes coated with the anti-coagulant, ethylenediaminetetra acetic acid (EDTA). The first tube was discarded to account for the skin plug and locally activated platelets resulting from the needle insertion. The blood vials were centrifuged at 150g for 15mins to separate the plasma from the red blood cells (erythrocytes). The plasma was then pooled into fresh tubes, and used within 2hrs.

2.5 Platelet adhesion and viability on PCL nanowire and nanofiber surfaces

Sterilized PCL, NW and NF surfaces were incubated in a 24-well plate with 1000μl of pooled plasma at room temperature on a horizontal shaker plate (100rpm) for 2hrs. The effects of the surface nanoarchitecture on platelets adhesion and viability were investigated and compared to that on the control surface.

Platelet adhesion was characterized by staining the cells with calcein-AM (Invitrogen) live stain. Prior to staining, the un-adhered platelets were removed by aspirating the plasma from the surfaces followed by rinsing with PBS. The surfaces were incubated with 2μM calcein-AM solution in PBS for 30mins on a horizontal shaker plate (100rpm) at room temperature. The surfaces were then rinsed with PBS and imaged with a fluorescence microscope using appropriate filters. Further, the fluorescence microscopy images were analyzed using ImageJ software to calculate the number of adhered platelets on surfaces.

Platelet viability was characterized using a commercially available MTT assay kit. Through the use of bicinchoninic acid (BCA), this assay detects the cuprous ion (Cu^{+1}), which forms when Cu^{+2} is reduced by protein. The chelation of two molecules of BCA with one cuprous ion forms a purple reaction product that exhibits a strong absorbance at 562nm. The production of Cu^{+1} is directly proportional to the concentration of the protein and the incubation time in BCA. Thus, protein concentration can be calculated using a standardized protein curve. Prior to measuring the MTT activity, the un-adhered platelets were removed by aspirating the plasma from the surfaces followed by rinsing with PBS. The nanostructured surfaces were incubated with 10% MTT solution in hepes-tyrode buffer for 4hrs on a horizontal shaker plate (100 rpm) at room temperature. The resulting formazan crystals were dissolved by adding MTT solvent in the amounts equal to the hepes-tyrode buffer. The absorbance of the solution was measured using a plate reader.

2.6 Platelet activation on PCL nanowire and nanofiber surfaces

Sterilized PCL, NW and NF surfaces were incubated in a 24-well plate with 1000μl of pooled plasma at room temperature on a horizontal shaker plate (100rpm) for 2hrs. Un-adhered platelets were removed by aspirating the plasma from the surfaces followed by rinsing with PBS. Platelet activation on nanostructured surfaces was visualized using SEM imaging. The platelets were fixed by incubating the surfaces in a solution of primary fixative (3% glutaraldehyde (Sigma), 0.1M sodium cacodylate (Polysciences), and 0.1M sucrose (Sigma) for 45mins. This was followed by incubation in a solution of secondary fixative (primary fixative without gluteraldehyde) for 2hrs. This was followed by a dehydration step where the surfaces were incubated in consecutive solutions of ethanol (35%, 50%, 70%, 95%, 100%) for 10mins. Further dehydration of the platelets was accomplished by incubating the surfaces in hexamethyldisilazane (HMDS, Sigma) for 10mins. The surfaces were coated with a 10nm layer of gold and imaged at 5–7kV. The SEM images were then used to determine the percentage of the adhered platelets that were unactivated, or had a short-dendritic or a long-dendritic morphology. The following scheme was used to determine the morphology of the adhered platelets:

- Unactivated: Platelets that are normal and with compact central body
- Short-dendritic: Platelets with smaller dendrites and partially activated
- Long-dendritic: Platelets with many long dendrites and completely activated

2.7 Whole blood clotting on PCL nanowire and nanofiber surfaces

Sterilized PCL, NW and NF surfaces were transferred to a 24-well plate to evaluate whole blood clotting kinetics. Whole human blood from healthy individuals was drawn, and 5μl of

the blood was immediately dropped on the surfaces. The blood was allowed to clot for up to 60mins, and the free hemoglobin concentration was measured at 15min intervals. In order to measure the free hemoglobin concentration, the surfaces were transferred into a different 24-well plate with 500μl of DI water. The surfaces were gently agitated for 30secs and left in the DI water for 5mins to release free hemoglobin from red blood cells that were not trapped in the thrombus. The absorbance of the DI water with free hemoglobin was measured at a wavelength of 540nm using a plate reader. The value of absorbance is directly proportional to the concentration of free hemoglobin in DI water. Further, the surfaces were air dried, coated with a 10nm layer of gold and imaged with SEM at 5–7kV.

2.8 Statistical analysis

Each experiment was reconfirmed on three different surfaces of each PCL, NW and NF with at least three different platelet populations ($n_{min} = 9$). The protein adsorption results were confirmed on three different surfaces of each PCL, NW and NF with at least two repetitions ($n_{min} = 6$). All the quantitative results were analyzed using t-test. Statistical significance was considered at $p < 0.05$.

3. RESULTS AND DISCUSSION

Current treatments for cardiovascular disease include organ transplants, surgery, metabolic products and mechanical/synthetic implants. However, rejection of cardiovascular implants continues to be a problem, eliciting a need for understanding the mechanisms behind tissue-material interaction. Recently, there has been an increased interest in exploring nanostructured surface topographies as interfaces for implantable devices. Several studies have reported favorable cellular response on such nanostructured topographies, however few studies report the hemocompatibility of these surfaces. In this work, we have evaluated the hemocompatibility of NW and NF surfaces fabricated by nano-templating method and electrospinning respectively.

3.1. Fabrication and characterization of PCL nanowire and nanofiber surfaces

In order to characterize the nanoarchitecture of the NW and NF surfaces, SEM imaging was used (Figure 1). Using the image analysis system built into the SEM system, the height and the diameter of the nanowires (Figure 1B and C) were computed to be 4.5 ± 0.5μm and 150 ± 50 nm respectively, while the diameter of the nanofibers was computed to be 290 ± 200 nm (Figure 1D and E). The images show that the NW surfaces have a uniform architecture with occasional interruption in the uniformity by the presence of random microchannels formed due to surface charge effects. Previous studies have shown that similar NW and NF surfaces enhance cellular functionality [57, 59, 60].

The hydrophilic nature of the nanostructured surfaces was characterized by contact angle measurements of DI water using a sessile drop measuring technique. The contact angle is defined as the angle between the surface and the tangent line at the point of contact of the DI water droplet with the surface [58]. The results indicate that the NW surfaces (71.9 ± 3.3°) are more hydrophilic compared to the NF surfaces (98.2°± 6.4°) and PCL surfaces surfaces (84.7 ± 1.5°) (Figure 2). Higher surface energy is associated with hydrophilic surfaces, whereas lower surface energy is associated with hydrophobic surfaces. Surface energy is defined as the product of surface area and the specific surface energy. Due to the fact that all three surfaces are fabricated from PCL, the specific surface energy is constant. Thus, the surface energy is solely dependent on the surface area. As evident from SEM images (Figure 1B and C), the NW surfaces have higher surface area compared to NF and PCL surfaces. Nanowires are aligned perpendicular to the surface while nanofibers are aligned parallel to the surface. This alteration in the alignment of nanostructures on the surface resulted in

higher surface area of NW surfaces compared to NF surfaces. Thus, NW surfaces have higher surface energy, resulting in a hydrophilic surface property. It is well known that the increased surface energy improves the interaction between the surface and the biological environment such as increased cell spreading on the surface [61].

3.2 Protein adsorption on PCL nanowire and nanofiber surfaces

When a biomaterial is implanted, proteins from the blood and surrounding tissue are adsorbed onto the surface within seconds to minutes Protein adsorption is an active process where the proteins may adsorb in differing quantities, densities, conformations and orientations depending on specific surface characteristics presented [62]. Further biological processes, such as activation of coagulation and inflammation cascades are impacted by the early adsorption of blood serum proteins. Therefore, the effect of protein adsorption on nanostructured surfaces is an important indicator of blood compatibility.

In this study, adsorption of key blood serum proteins, ALB, FIB and IgG was assessed on nanostructured surfaces. ALB is the main protein in blood plasma that functions mainly to regulate and maintain colloidal osmotic pressure of blood. It is a globular protein and may be distorted upon interaction with the surface [62]. FIB is a plasma glycoprotein that plays a key role in the inflammatory response by assisting in clot formation. It forms a Y shaped structure with two identical halves (F_{ab}) linked by a globular domain in the center (F_c) [62]. IgG is the main antibody isotype found in the blood that functions to control infection of body tissues. It also exhibits a Y shaped formation, similar to that of FIB, however it is not as elongated as FIB. The amount of protein adhered on the surfaces were determined using two different methods: a micro-BCA assay and XPS surface analysis. The micro-BCA assay was used to measure the total protein adsorption (bulk plus surface), whereas XPS was used to measure the surface protein adsorption. The adsorbed proteins on the nanostructured surfaces were further visualized using SEM.

In order to evaluate the total protein adsorption, the proteins adsorbed on the surfaces were desorbed using an anionic detergent, SDS and their amounts were evaluated using micro-BCA assay. The results indicate no significant differences in ALB adsorption on all the surfaces (Figure 3). However, FIB and IgG adsorbed significantly more on NW, followed by PCL surfaces and NF surfaces.

In order to evaluate the surface protein adsorption, high-resolution C1s scans were taken using XPS. The high resolution C1s peak consists of three sub-peaks: C-C, C-N and N-C=O. A precise way to characterize proteins adsorbed on the surface is to determine the contribution of N-C=O (amide) peak (the N-C=O peaks is at a shift 1.8eV from the C-C peak) in the overall C1s peak. (Figure 4 and Table 1). The results indicate that all the three surfaces had similar contribution of N-C=O peak for ALB adsorption, indicating similar amounts of ALB adsorbed on all the surfaces. However, NF surfaces had higher contribution of N-C=O peak for both FIB and IgG adsorption, indicating higher FIB and IgG adsorption compared to that on NW and PCL surfaces.

The results obtained from XPS are in contrast with that from micro-BCA assay. This can be explained based on variations in the surface nanotopography as well as the structure of the protein and how it is adsorbed on different nanostructured surfaces. It is evident from SEM images (Figure 1) that nanostructured surfaces at a nanoscale level can be considered to have a three-dimensional structure. In case of NW surfaces, this three-dimensional structure can be visualized due to the presence of gaps between the individual nanowires as well as the microchannels that are formed due to the surface tension interaction during the membrane dissolution process. The proteins will not only adsorb on the surface of nanowires, but also may penetrate through the three-dimensional structure and adsorb into

the gaps and the microchannels. In case of NF surfaces, the three-dimensional structure can be visualized as an interconnected porous network formed by continuous nanofibers that are present through the bulk of the substrate. The proteins will not only adsorb on the surface of NF, but also may infiltrate into the interconnected porous network and adsorb on the fibers beneath the surface. In case of PCL surfaces, the lack of any surface nanoarchitecture limits the proteins adsorption to the surface.

The results indicate that total as well as surface ALB adsorption was similar on all three nanostructured surfaces. ALB is a globular protein that is typically more hydrophobic than hydrophilic [63]. This may prevent the protein molecules from infiltrating into the three-dimensional structure of the nanostructured surfaces. Thus, all the ALB adsorbed on the surface similar to that of the PCL surface. This resulted in similar trends in total and surface ALB adsorption on nanostructured surfaces. In contrast, FIB and IgG adsorption was different on different surfaces. Further, the results indicate that NW surfaces had higher total FIB and IgG adsorption compared to NF and PCL surfaces. In contrast, NW surface had lower surface FIB and IgG adsorption compared to NF and PCL surfaces. This can be explained based on the structure of FIB and IgG as well as the ability of the surfaces to allow protein infiltration. Both FIB and IgG have a planar Y shape structure, with FIB being more elongated then IgG. Studies have shown that FIB [62] and F_c portion of IgG [64–66] is more attracted to hydrophobic surfaces. Due to the Y shape structure of both FIB and IgG as well their tendency to be less attracted towards hydrophilic surfaces, the protein molecules will adsorb less on the NW surfaces. However, the protein molecules may still penetrate through the three-dimensional structure and adsorb into the gaps and the microchannels, resulting in higher total protein adsorption on NW surfaces due to the availability of higher surface area for protein molecules to interact. In contrast, NF surfaces are more hydrophobic then NW surfaces, resulting in higher surface FIB and IgG adsorption. However, due to the interconnected porous network formed by continuous nanofibers and the Y shape of both FIB and IgG, the protein molecules may not be able to infiltrate that easily into the three-dimensional structure, resulting in lower total FIB and IgG adsorption on NF surfaces as compared to NW surfaces. In case of PCL surfaces, the lack of nanotopography resulted in all the protein adsorbed on the surface and total protein adsorption is equal to the surface protein adsorption.

Adsorbed proteins on the nanostructured surfaces were also visualized using SEM (Figure 5). As expected, all the proteins that were adsorbed on PCL surfaces crystalized, whereas, the proteins adsorption was uniform on both NW and NF surfaces. This may be due to the fact that both surfaces have significantly higher surface area as compared to PCL surfaces.

3.3 Platelet adhesion and viability on PCL nanowire and nanofiber surfaces

Platelet adhesion on a surface triggers the coagulation of blood and therefore is an important indicator of thrombogenecity. In this study, platelets were isolated from whole human blood and their adhesion on nanostructured surfaces was investigated after 2hrs of contact time. The platelets were stained with calcein-AM and the surfaces were examined under a fluorescence microscope to evaluate the platelet adhesion. The results indicate significantly higher platelet adhesion on NF surfaces followed by PCL surfaces and NW surfaces (Figure 6). Further, high-magnification images reveal that platelets are clustering and probably infiltrating in the NF surfaces (Figure 6G, H and I). In contrast, the platelets on PCL and NW surfaces do not form clusters (Figure 6 PCL: A, B and C; NW: D, E and F).

Further, low magnification (10x) fluorescence microscopy images were analyzed using ImageJ software to determine the number of platelets adhered on different surfaces. The results indicate significantly higher platelet adhesion on NF surfaces followed by PCL surfaces and NW surfaces (Figure 7). Platelet adhesion results were consistent with the

protein adsorption results. The NF surfaces had higher surface FIB adsorption compared to PCL and NW surfaces resulting in higher platelet adhesion. This is consistent with recent work demonstrating higher platelet adhesion and activation on NF surfaces [67].

Platelet viability was evaluated using an MTT assay. The MTT assay determines the amount of mitochondrial activity in the live cells via dehydrogenase activity. This assay measures the absorbance of formazan, which is reduced by MTT in living cells. Therefore, the amount of adhered platelets directly corresponds to the absorbance values of formazan. The results indicate significantly higher platelet viability on NF surfaces as compared to PCL and NW surfaces, indicating higher number of platelets present on NF surfaces (Figure 8). These results also validate the results obtained from fluorescence microscopy.

3.4 Platelet activation on PCL nanowire and nanofiber surfaces

Once plasma proteins adsorb on a biomaterial surface, a series of biochemical events that cause platelet adhesion and activation is initiated. Activated platelets trigger the activation of plasma coagulation factors which lead to the generation of a fibrin clot [68]. Platelet activation after 2hrs of contact time with nanostructured surfaces was investigated with SEM imaging. The nanostructured surfaces were coated with a 10nm layer of gold and imaged at 5–7kV. The SEM images at low magnifications indicate significantly higher number of platelets on NF surfaces followed by PCL surfaces and NW surfaces (Figure 9). These results are in conjunction with fluorescence microscopy images as well as MTT assay.

High magnification SEM images reveal significant morphological differences in platelets adhered on the different surfaces. The SEM images were used to determine the percentage of adhered platelets that were unactivated or had a dendritic (short-dendritic or long-dendritic) morphology (Figure 10). The results show NF surfaces with a higher percentage of platelets with long-dendritic morphology (~50%) indicating complete activation, followed by platelets with short-dendritic morphology (~30%), and fewer platelets with unactivated morphology (~20%). In contrast, PCL surfaces has higher percentage of platelets with short-dendritic morphology (~56%), followed by platelets with unactivated morphology (~23%), and fewer platelets that are completely activated (~21%). NW surfaces has higher percentage of platelets with unactivated morphology (~55%), followed by platelets with short-dendritic morphology (~27%), and fewer platelets exhibiting long-dendritic morphology (~17%). It is important to note that PCL and NW surfaces can potentially activate platelets as the clotting cascade progresses despite the fact that they do not support significant platelet adhesion. Furthermore, these results indicate the importance of surface topography in influencing the platelet activation on the material surface.

3.5 Whole blood clotting on PCL nanowire and nanofiber surfaces

Following platelet adhesion and activation, the next step in the cascade of blood coagulation is the formation of a fibrin matrix. The kinetics of whole blood clotting is important in determining the success of a long-term blood contacting material. If a clot forms abruptly tissue integration will be inhibited. The results indicated that blood clotted on all surfaces within 1hr of exposure, however the rate of clotting was different for different surfaces (Figure 11). After 30mins of clotting, there were significant differences in the amount of free hemoglobin in the blood that was in contact with NW surfaces indicating least clotting on the surface, followed by NF and PCL surfaces. Further, increased amounts of free hemoglobin were in the blood that was in contact with NW surfaces compared to both PCL and NF surfaces throughout the entire clotting process. These results are consistent with platelet activation studies as well as surface FIB adsorption.

The blood clotting cascade is initiated by the enzyme thrombin, which converts fibrinogen into fibrin, eventually forming a clot network. The fibrin network after 60mins of clotting time on PCL, NW and NF surfaces was examined using SEM imaging. Visual inspections show the fibrin matrix formation to be altered on all three surfaces (Figure 12). Due to the hydrophobic nature of PCL surfaces, the blood drop did not spread when it contact with the surface, resulting in well-defined blood-PCL interface (Figure 12A, B and C). In contrast, due to the hydrophilic nature of the NW surface, the blood drop spread on the surface and infiltrated the nanoarchitecture, resulting in a “gradient-like” blood-NW interface (Figure 12D, E and F). However, due to the porous nature of NF surfaces, the blood drop completely infiltrated in the surface without any trace of blood-NF interface (Figure 12G, H and I).

4. CONCLUSION

Recently, there has been an increased interest in exploring nanostructured surface topographies as interfaces for implantable devices. Several studies have reported favorable cellular response on different nanostructured topographies, however few studies report the hemocompatibility of these surfaces. In this work, we have evaluated the hemocompatibility of NW and NF surfaces fabricated by nano-templating method and electrospinning respectively. The results indicate no significant differences in ALB adsorption on all surfaces. However, NW surfaces had higher total FIB and IgG adsorption compared to NF and PCL surfaces. In contrast, NW surfaces had lower surface FIB and IgG adsorption compared to NF and PCL surfaces. This can be explained based on the structure of FIB and IgG as well as the ability of the surfaces to allow protein infiltration. Platelet adhesion and viability studies show a large amount of adhesion and clustering of platelets on the NF surfaces as compared to PCL and NW surfaces. Platelet activation studies reveal that NW surfaces have the highest percentage of unactivated platelets, whereas NF surfaces have the highest percentage of fully activated platelets. Whole blood clotting results indicate that NW surfaces maintain an increased amount of free hemoglobin during the clotting process compared to PCL and NF surface, indicating less clotting and slower rate of clotting on their surfaces. The results presented here indicate that the surface nanoarchitecture and how it is presented to the biological environment can modulate the hemocompatibility. Further studies are now directed towards evaluating the effects of altered lengths and diameters of nanofeatures on hemocompatibility and specific components of the innate immune response.

Acknowledgments

Research reported in this publication was supported by the National Institute of Arthritis and Musculoskeletal and Skin Diseases of the National Institutes of Health under Award Number 5-R21-AR057341-02. The content is solely the responsibility of the authors and does not necessarily represent the official views of the National Institutes of Health.

REFERNCES

1. Smith SC Jr. Our time: A call to save preventable death from cardiovascular disease (heart disease and stroke). Journal of the American College of Cardiology. 2012; 60(22):2343–2348. [PubMed: 22995536]
2. Nugent HM, Edelman ER. Tissue Engineering Therapy for Cardiovascular Disease. Circulation Research. 2003; 92:1068–78. [PubMed: 12775655]
3. Seyednejad H, Gawlitta D, Kuiper RV, de Bruin A, van Nostrum CF, Vermonden T, et al. In vivo biocompatibility and biodegradation of 3D-printed porous scaffolds based on a hydroxyl-functionalized poly(ε-caprolactone). Biomaterials. 2012; 33:4309–18. [PubMed: 22436798]
4. Heublein B, Rohde R, Kaese V, Niemeyer M, Hartung W, Haverich A. Biocorrosion of magnesium alloys: a new principle in cardiovascular implant technology? Heart. 2003; 89:651–6. [PubMed: 12748224]

5. van der Giessen WJ, Lincoff AM, Schwartz RS, van Beusekom HMM, Serruys PW, Holmes DR, et al. Marked Inflammatory Sequelae to Implantation of Biodegradable and Nonbiodegradable Polymers in Porcine Coronary Arteries. Circulation. 1996; 94:1690–7. [PubMed: 8840862]
6. Zhang Y, Ouyang H, Lim CT, Ramakrishna S, Huang Z-M. Electrospinning of gelatin fibers and gelatin/PCL composite fibrous scaffolds. Journal of Biomedical Materials Research Part B: Applied Biomaterials. 2005; 72B:156–65.
7. Ajili SH, Ebrahimi NG, Soleimani M. Polyurethane/polycaprolactane blend with shape memory effect as a proposed material for cardiovascular implants. Acta Biomaterialia. 2009; 5:1519–30. [PubMed: 19249261]
8. Kim HI, Ishihara K, Lee S, Seo J-H, Kim HY, Suh D, et al. Tissue response to poly(l-lactic acid)-based blend with phospholipid polymer for biodegradable cardiovascular stents. Biomaterials. 2011; 32:2241–7. [PubMed: 21185597]
9. Shinoka T, Ma PX, Shum-Tim D, Breuer CK, Cusick RA, Zund G, et al. Tissue-engineered heart valves. Autologous valve leaflet replacement study in a lamb model. Circulation. 1996; 94:II164–8. [PubMed: 8901739]
10. Andukuri A, Kushwaha M, Tambralli A, Anderson JM, Dean DR, Berry JL, et al. A hybrid biomimetic nanomatrix composed of electrospun polycaprolactone and bioactive peptide amphiphiles for cardiovascular implants. Acta Biomaterialia. 2011; 7:225–33. [PubMed: 20728588]
11. Motlagh D, Allen J, Hoshi R, Yang J, Lui K, Ameer G. Hemocompatibility evaluation of poly(diol citrate) in vitro for vascular tissue engineering. Journal of Biomedical Materials Research Part A. 2007; 82A:907–16. [PubMed: 17335023]
12. Belanger MC, Marois Y, Roy R, Mehri Y, Wagner E, Zhang Z, et al. Selection of a polyurethane membrane for the manufacture of ventricles for a totally implantable artificial heart: Blood compatibility and biocompatibility studies. Artificial Organs. 2000; 24:879–88. [PubMed: 11119076]
13. Maegdefessel L, Linde T, Krapiec F, Hamilton K, Steinseifer U, van Ryn J, et al. In vitro comparison of dabigatran, unfractionated heparin, and low-molecular-weight heparin in preventing thrombus formation on mechanical heart valves. Thrombosis Research. 2010; 126:e196–e200. [PubMed: 20659761]
14. Motlagh D, Yang J, Lui KY, Webb AR, Ameer GA. Hernocompatibility evaluation of poly(glycerol-sebacate) in vitro for vascular tissue engineering. Biomaterials. 2006; 27:4315–24. [PubMed: 16675010]
15. Baker DW, Liu X, Weng H, Luo C, Tang L. Fibroblast/Fibrocyte: Surface Interaction Dictates Tissue Reactions to Micropillar Implants. Biomacromolecules. 2011; 12:997–1005. [PubMed: 21332193]
16. Muthusubramaniam L, Lowe R, Fissell W, Li L, Marchant R, Desai T, et al. Hemocompatibility of Silicon-Based Substrates for Biomedical Implant Applications. Annals of Biomedical Engineering. 2011; 39:1296–305. [PubMed: 21287275]
17. Huang N, Yang P, Leng YX, Chen JY, Sun H, Wang J, et al. Hemocompatibility of titanium oxide films. Biomaterials. 2003; 24:2177–87. [PubMed: 12699653]
18. Feng Y, Zhao H, Zhang L, Guo J. Surface modification of biomaterials by photochemical immobilization and photograft polymerization to improve hemocompatibility. Frontiers of Chemical Engineering in China. 2010; 4:372–81.
19. Werner C, Maitz MF, Sperling C. Current strategies towards hemocompatible coatings. Journal of Materials Chemistry. 2007; 17:3376–84.
20. Ziats NP, Miller KM, Anderson JM. In vitro and in vivo interactions of cells with biomaterials. Biomaterials. 1988; 9:5–13. [PubMed: 3280039]
21. Anderson JM, McNally AK. Biocompatibility of implants: lymphocyte/macrophage interactions. Semin Immunopathol. 2011; 33:221–33. [PubMed: 21271251]
22. André P, Delaney SM, LaRocca T, Vincent D, DeGuzman F, Jurek M, et al. P2Y12 regulates platelet adhesion/activation, thrombus growth, and thrombus stability in injured arteries. The Journal of Clinical Investigation. 2003; 112:398–406. [PubMed: 12897207]

23. Cerda-Cristerna BI, Flores H, Pozos-Guillén A, Perez E, Sevrin C, Grandfils C. Hemocompatibility assessment of poly(2-dimethylamino ethylmethacrylate) (PDMAEMA)-based polymers. Journal of Controlled Release. 2011; 153:269–77. [PubMed: 21550368]
24. Major TC, Brant DO, Burney CP, Amoako KA, Annich GM, Meyerhoff ME, et al. The hemocompatibility of a nitric oxide generating polymer that catalyzes S-nitrosothiol decomposition in an extracorporeal circulation model. Biomaterials. 2011; 32:5957–69. [PubMed: 21696821]
25. Cerda-Cristerna BI, Flores H, Pozos-Guillen A, Perez E, Sevrin C, Grandfils C. Hemocompatibility assessment of poly(2-dimethylamino ethylmethacrylate) (PDMAEMA)-based polymers. Journal of Controlled Release. 2011; 153:269–77. [PubMed: 21550368]
26. de Jonge L, Leeuwenburgh S, Wolke J, Jansen J. Organic–Inorganic Surface Modifications for Titanium Implant Surfaces. Pharmaceutical Research. 2008; 25:2357–69. [PubMed: 18509601]
27. Ishihara K, Oshida H, Endo Y, Ueda T, Watanabe A, Nakabayashi N. Hemocompatibility of human whole blood on polymers with a phospholipid polar group and its mechanism. Journal of Biomedical Materials Research. 1992; 26:1543–52. [PubMed: 1484061]
28. Ekblad T, Liedberg B. Protein adsorption and surface patterning. Current Opinion in Colloid & Interface Science. 2010; 15:499–509.
29. Faria M, Brogueira P, de Pinho MN. Sub-micron tailoring of bi-soft segment asymmetric polyurethane membrane surfaces with enhanced hemocompatibility properties. Colloids and Surfaces B-Biointerfaces. 2011; 86:21–7.
30. Kim HN, Jiao A, Hwang NS, Kim MS, Kang DH, Kim D-H, et al. Nanotopography-guided tissue engineering and regenerative medicine. Advanced Drug Delivery Reviews. In press.
31. Cao H, McHugh K, Chew SY, Anderson JM. The topographical effect of electrospun nanofibrous scaffolds on the in vivo and in vitro foreign body reaction. Journal of Biomedical Materials Research Part A. 2010; 93A:1151–9. [PubMed: 19768795]
32. Bechara S, Wadman L, Popat KC. Electroconductive polymeric nanowire templates facilitates in vitro C17. 2 neural stem cell line adhesion, proliferation and differentiation. Acta Biomaterialia. 2011; 7:2892–901. [PubMed: 21530693]
33. McMurray RJ, Gadegaard N, Tsimbouri PM, Burgess KV, McNamara LE, Tare R, et al. Nanoscale surfaces for the long-term maintenance of mesenchymal stem cell phenotype and multipotency. Nat Mater. 2011; 10:637–44. [PubMed: 21765399]
34. Park K, Ju YM, Son JS, Ahn KD, Han DK. Surface modification of biodegradable electrospun nanofiber scaffolds and their interaction with fibroblasts. J Biomater Sci Polym Ed. 2007; 18:369–82. [PubMed: 17540114]
35. Seidlits SK, Lee JY, Schmidt CE. Nanostructured scaffolds for neural applications. Nanomedicine. 2008; 3:183–99. [PubMed: 18373425]
36. Bechara SL, Judson A, Popat KC. Template synthesized poly(epsilon-caprolactone) nanowire surfaces for neural tissue engineering. Biomaterials. 2010; 31:3492–501. [PubMed: 20149440]
37. Woodruff MA, Hutmacher DW. The return of a forgotten polymer—Polycaprolactone in the 21st century. Progress in Polymer Science. 2010; 35:1217–56.
38. Liu L, Guo SR, Chang J, Ning CQ, Dong CM, Yan DY. Surface modification of polycaprolactone membrane via layer-by-layer deposition for promoting blood compatibility. Journal of Biomedical Materials Research Part B-Applied Biomaterials. 2008; 87B:244–50.
39. Xiang P, Li M, Zhang CY, Chen DL, Zhou ZH. Cytocompatibility of electrospun nanofiber tubular scaffolds for small diameter tissue engineering blood vessels. International Journal of Biological Macromolecules. 2011; 49:281–8. [PubMed: 21600916]
40. Li WJ, Cooper JA, Mauck RL, Tuan RS. Fabrication and characterization of six electrospun poly(alpha-hydroxy ester)-based fibrous scaffolds for tissue engineering applications. Acta Biomaterialia. 2006; 2:377–85. [PubMed: 16765878]
41. De Santis R, Gloria A, Russo T, D'Amora U, Zeppetelli S, Dionigi C, et al. A Basic Approach Toward the Development of Nanocomposite Magnetic Scaffolds for Advanced Bone Tissue Engineering. Journal of Applied Polymer Science. 2011; 122:3599–605.
42. Sangsanoh P, Waleetorncheepsawat S, Suwantong O, Wutticharoenmongkol P, Weeranantanapan O, Chuenjitbuntaworn B, et al. In vitro biocompatibility of schwann cells on surfaces of

biocompatible polymeric electrospun fibrous and solution-cast film scaffolds. Biomacromolecules. 2007; 8:1587–94. [PubMed: 17429941]

43. Cooper A, Bhattarai N, Zhang MQ. Fabrication and cellular compatibility of aligned chitosan-PCL fibers for nerve tissue regeneration. Carbohydrate Polymers. 2011; 85:149–56.
44. Lee W, Oh JH, Park JC, Shin HI, Baek JH, Ryoo HM, et al. Performance of electrospun poly(epsilon-caprolactone) fiber meshes used with mineral trioxide aggregates in a pulp capping procedure. Acta Biomater. 2012; 8:2986–95. [PubMed: 22542886]
45. Ng KW, Khor HL, Hutmacher DW. In vitro characterization of natural and synthetic dermal matrices cultured with human dermal fibroblasts. Biomaterials. 2004; 25:2807–18. [PubMed: 14962559]
46. Lam CX, Hutmacher DW, Schantz JT, Woodruff MA, Teoh SH. Evaluation of polycaprolactone scaffold degradation for 6 months in vitro and in vivo. J Biomed Mater Res A. 2009; 90:906–19. [PubMed: 18646204]
47. Christopher XFL, Monica MS, Swee-Hin T, Dietmar WH. Dynamics of in vitro polymer degradation of polycaprolactone-based scaffolds: accelerated versus simulated physiological conditions. Biomedical Materials. 2008; 3:034108. [PubMed: 18689929]
48. Sachlos E, Czernuszka JT. Making tissue engineering scaffolds work. Review: the application of solid freeform fabrication technology to the production of tissue engineering scaffolds. Eur Cell Mater. 2003; 5:29–39. [PubMed: 14562270]
49. Bechara SL, Judson A, Popat KC. Template synthesized poly(ε-caprolactone) nanowire surfaces for neural tissue engineering. Biomaterials. 2010; 31:3492–501. [PubMed: 20149440]
50. Redenti S, Tao S, Yang J, Gu P, Klassen H, Saigal S, et al. Retinal tissue engineering using mouse retinal progenitor cells and a novel biodegradable, thin-film poly(e-caprolactone) nanowire scaffold. Journal of Ocular Biology, Diseases, and Informatics. 2008; 1:19–29.
51. He L, Liu B, Xipeng G, Xie G, Liao S, Quan D, et al. Microstructure and properties of nano-fibrous PCL-b-PLLA scaffolds for cartilage tissue engineering. Eur Cell Mater. 2009; 18:63–74. [PubMed: 19859871]
52. Mavis B. Compartmentalization of synthetic body fluid constituents for coating electrospun PCL nanofiber mats with different calcium phosphate phases. Journal of Biomechanics. 2011; 44(Supplement 1):7.
53. Ye L, Wu X, Mu Q, Chen B, Duan Y, Geng X, et al. Heparin-Conjugated PCL Scaffolds Fabricated by Electrospinning and Loaded with Fibroblast Growth Factor 2. J Biomater Sci Polym Ed. 2010; 21:21.
54. Ye L, Wu X, Duan H-Y, Geng X, Chen B, Gu Y-Q, et al. The in vitro and in vivo biocompatibility evaluation of heparin–poly(ε-caprolactone) conjugate for vascular tissue engineering scaffolds. Journal of Biomedical Materials Research Part A. 2012; 100A:3251–8. [PubMed: 22733560]
55. Murugan R, Ramakrishna S. Nano-featured scaffolds for tissue engineering: a review of spinning methodologies. Tissue Eng. 2006; 12:435–47. [PubMed: 16579677]
56. Popat KC, Porter JR, Henson A. Biodegradable poly(epsilon-caprolactone) nanowires for bone tissue engineering applications. Biomaterials. 2009; 30:780–8. [PubMed: 19012962]
57. Ruckh TT, Kumar K, Kipper MJ, Popat KC. Osteogenic differentiation of bone marrow stromal cells on poly(epsilon-caprolactone) nanofiber scaffolds. Acta Biomaterialia. 2010; 6:2949–59. [PubMed: 20144747]
58. Popat KC, Johnson RW, Desai TA. Characterization of vapor deposited poly (ethylene glycol) films on silicon surfaces for surface modification of microfluidic systems. Journal of Vacuum Science & Technology B. 2003; 21:645–54.
59. Bechara SL, Judson A, Popat KC. Template synthesized poly(e-caprolactone) nanowire surfaces for neural tissue engineering. Biomaterials. 2010; 31:10.
60. Porter JR, Henson A, Popat KC. Biodegradable poly(ε-caprolactone) nanowires for bone tissue engineering applications. Biomaterials. 2009; 30:780–8. [PubMed: 19012962]
61. Zhao G, Schwartz Z, Wieland M, Rupp F, Geis-Gerstorfer J, Cochran DL, et al. High surface energy enhances cell response to titanium substrate microstructure. Journal of Biomedical Materials Research Part A. 2005; 74A:49–58. [PubMed: 15924300]

62. Roach P, Farrar D, Perry CC. Interpretation of Protein Adsorption: Surface-Induced Conformational Changes. Journal of the American Chemical Society. 2005; 127:8168–73. [PubMed: 15926845]

63. XMH, DCC. Atomic structure and chemistry of human serum albumin. Nature. 1992 Jul 16; 358(6383):209–15. [PubMed: 1630489]

64. Buijs J, van den Berg PAW, Lichtenbelt JWT, Norde W, Lyklema J. Adsorption Dynamics of IgG and Its F(ab′)2and Fc Fragments Studied by Reflectometry. Journal of Colloid and Interface Science. 1996; 178:594–605.

65. van Erp R, Linders YE, van Sommeren AP, Gribnau TC. Characterization of monoclonal antibodies physically adsorbed onto polystyrene latex particles. J Immunol Methods. 1992; 152:191–9. [PubMed: 1500729]

66. Nagaoka S, Kanno M, Kawakami H, Kubota S. Evaluation of blood compatibility of fluorinated polyimide by immunolabeling assay. J Artif Organs. 2001; 4:107–12.

67. Wan L-S, Xu Z-K. Polymer surfaces structured with random or aligned electrospun nanofibers to promote the adhesion of blood platelets. Journal of Biomedical Materials Research Part A. 2009; 89A:168–75. [PubMed: 18431780]

68. Heemskerk JW, Bevers EM, Lindhout T. Platelet activation and blood coagulation. 2002; 88(2): 186–93.

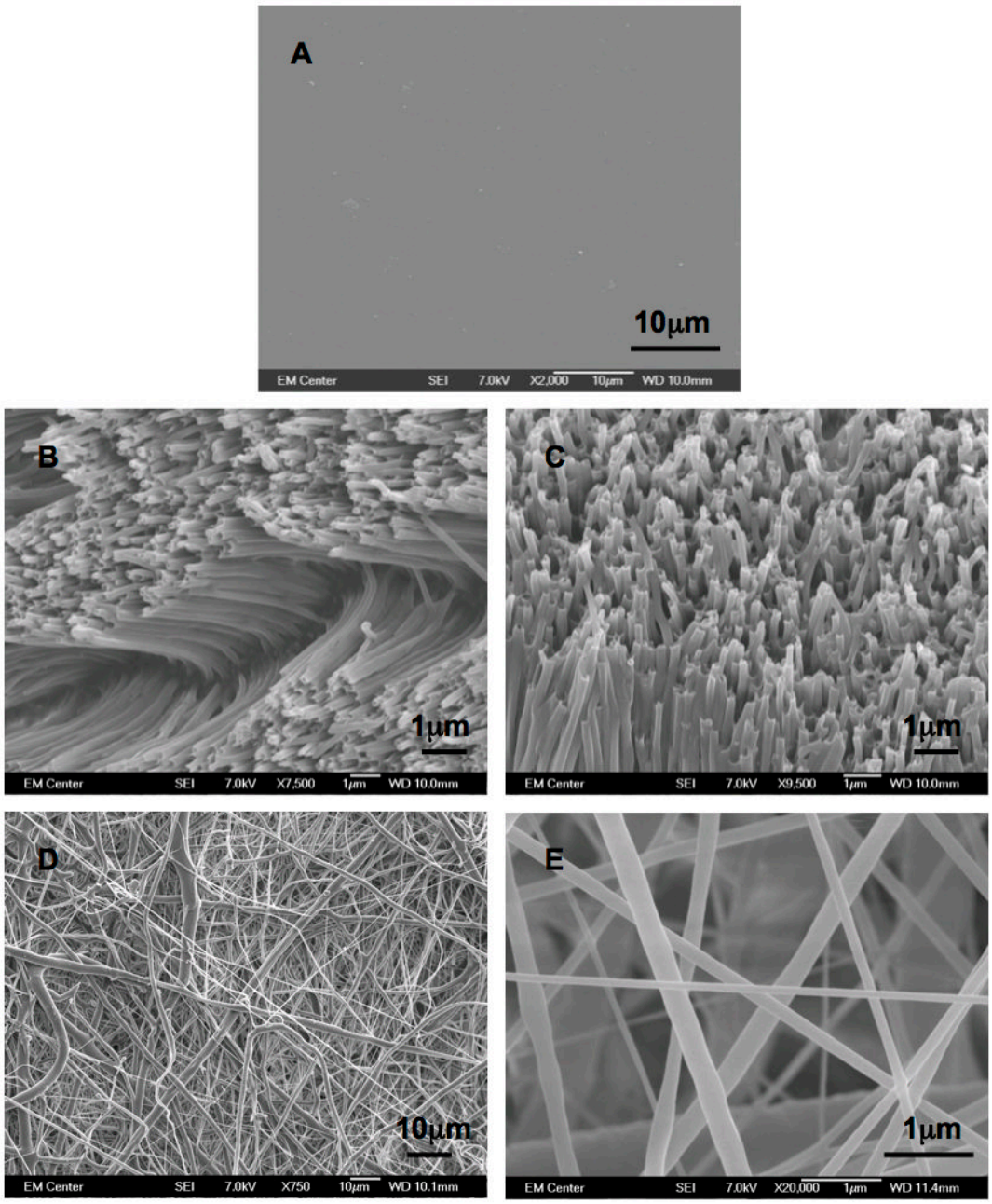

Figure 1.
Representative SEM images of (A) PCL, (B and C) NW and (D and E) NF surfaces.

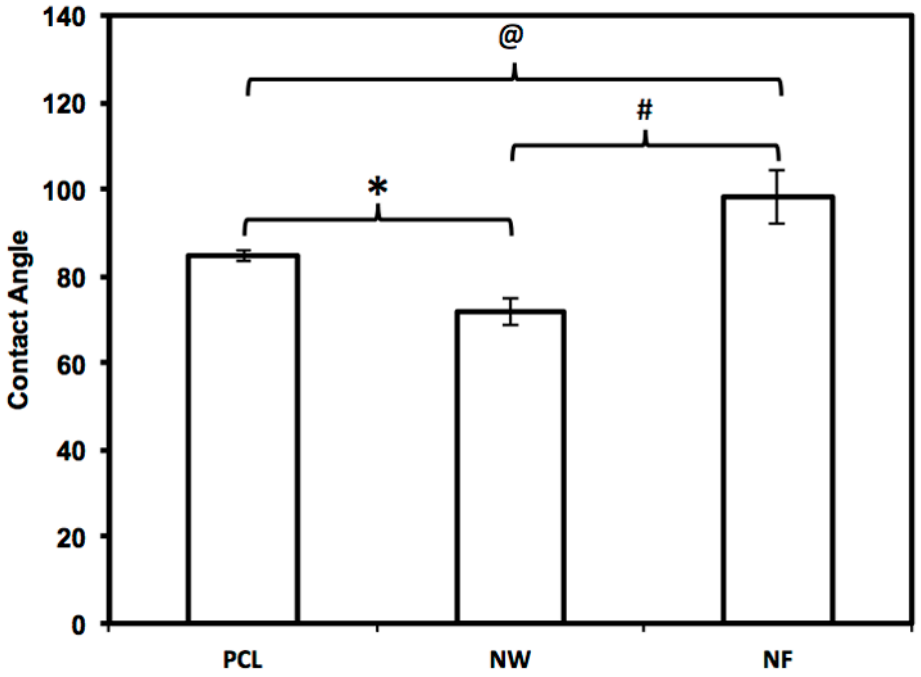

Figure 2.
Contact angle measurements of PCL, NW and NF surfaces indicating hydrophillic/ hydrophobic nature of the surfaces. Significantly different contact angle measurements were seen on all three surfaces (@, #, * → $p < 0.05$).

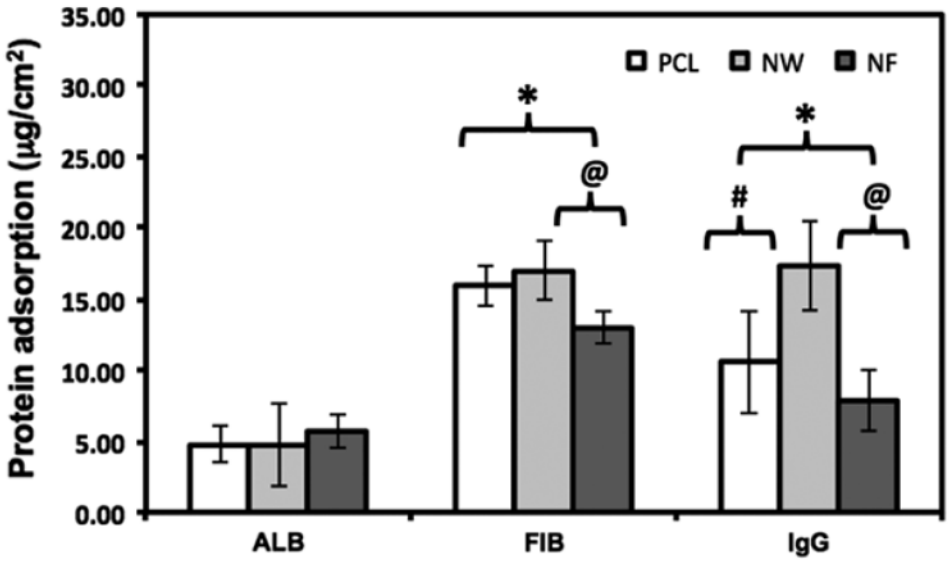

Figure 3.

Overall blood serum protein adsorption on PCL, NW and NF surfaces determined by micro-BCA assay. Note: No significant differences in ALB adsorption on PCL, NW and NF surfaces. Significant differences in FIB adsorption on PCL and NF surfaces, and NW and NF surfaces ($p < 0.05$). Significant differences in IgG adsorption on all surfaces ($p < 0.05$).

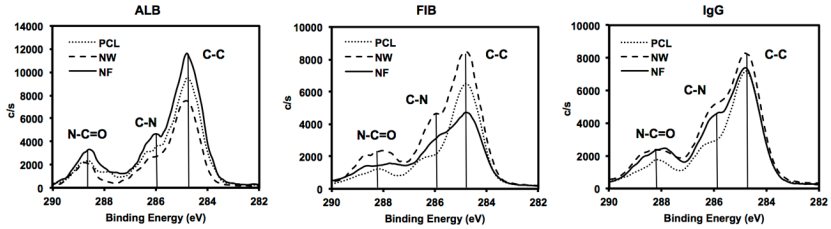

Figure 4.
High resolution C1s scans for surfaces adsorbed blood serum proteins on PCL, NW and NF surfaces showing C-C, C-N and N-C=O for ALB, FIB and IgG.

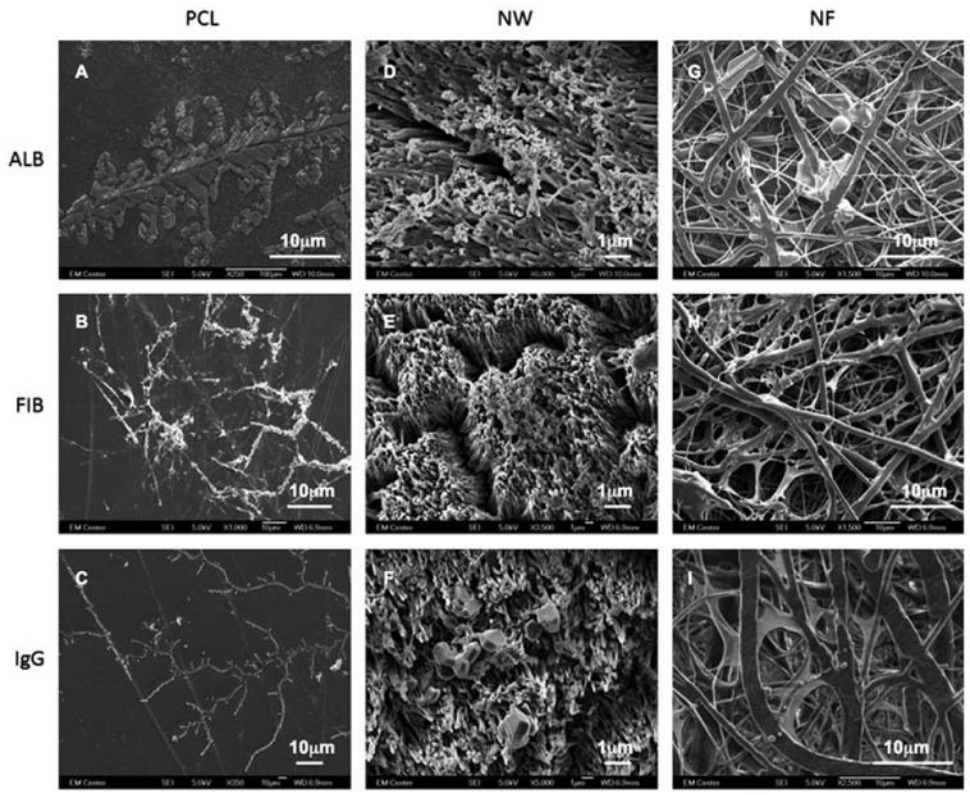

Figure 5.
Representative SEM images of ALB (A, D and G), FIB (B, E and H) and IgG (C, F and I) adsorbed on on PCL (A, B and C), NW (D, E and F) and NF (G, H and I) surfaces.

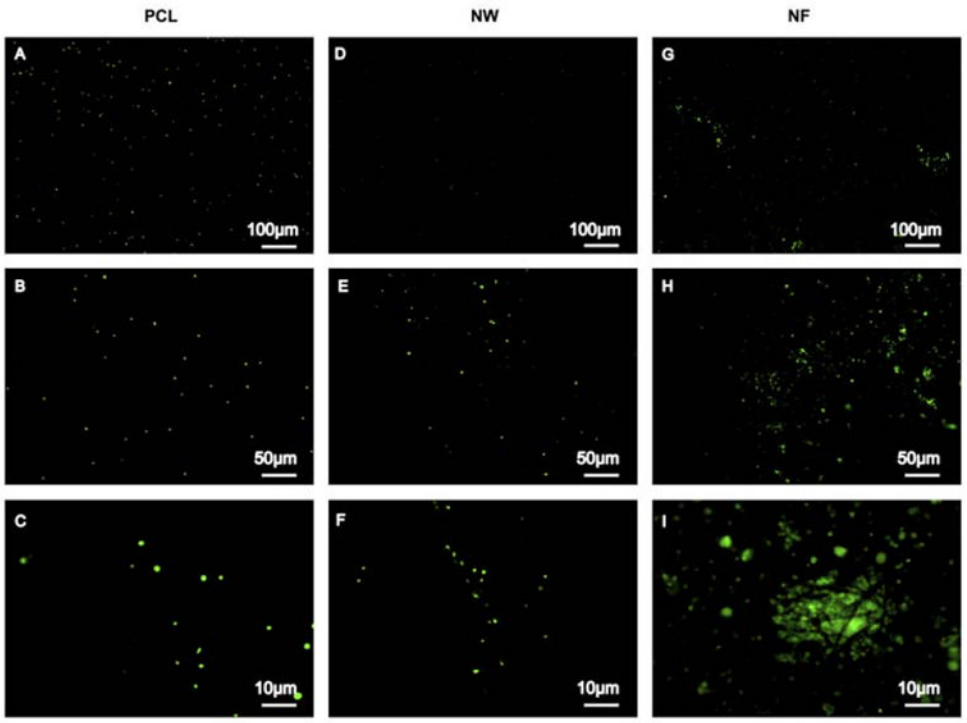

Figure 6.
Representative fluorescence microscopy images of adhered platelets stained with calcein-AM on PCL (A, B and C), NW (D, E and F) and NF (G, H and I) surfaces.

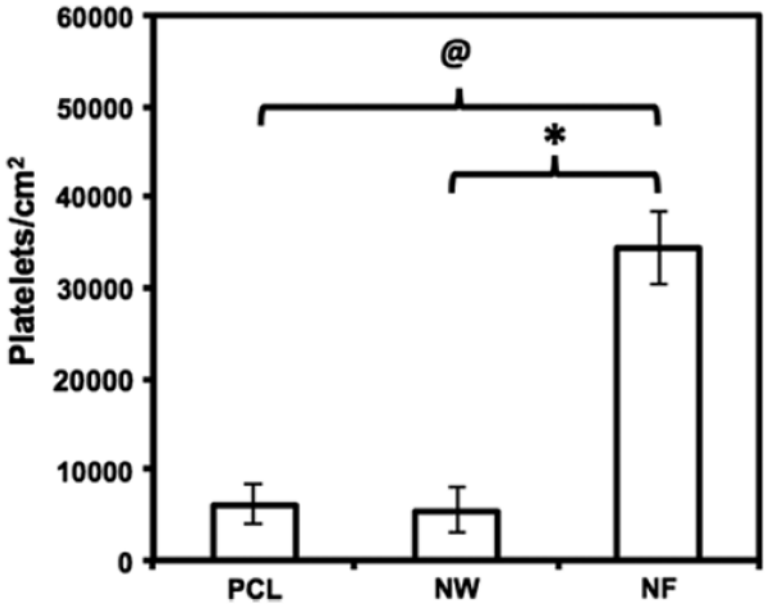

Figure 7.

Number of adhered platelets on PCL, NW and NF surfaces calculated using fluorescence microscopy images and ImageJ software. Significant differences in number of platelets adhered on PCL and NF surfaces (@→ $p < 0.05$), and NW and NF surfaces (* → $p < 0.05$).

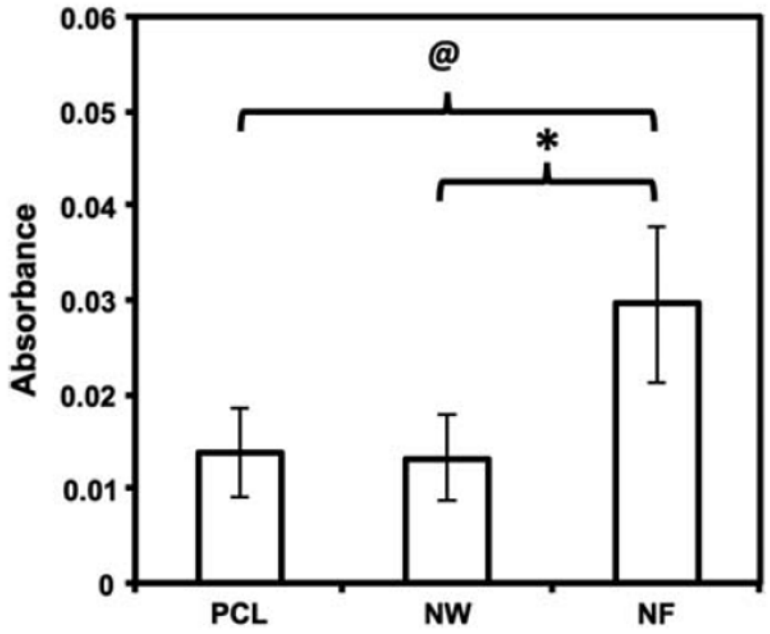

Figure 8.
MTT assay results indicating viability of adhered platelets on PCL, NW and NF surfaces. Significant differences in viability of platelets adhered on PCL and NF surfaces (@→ $p < 0.05$), and NW and NF surfaces (* → $p < 0.05$).

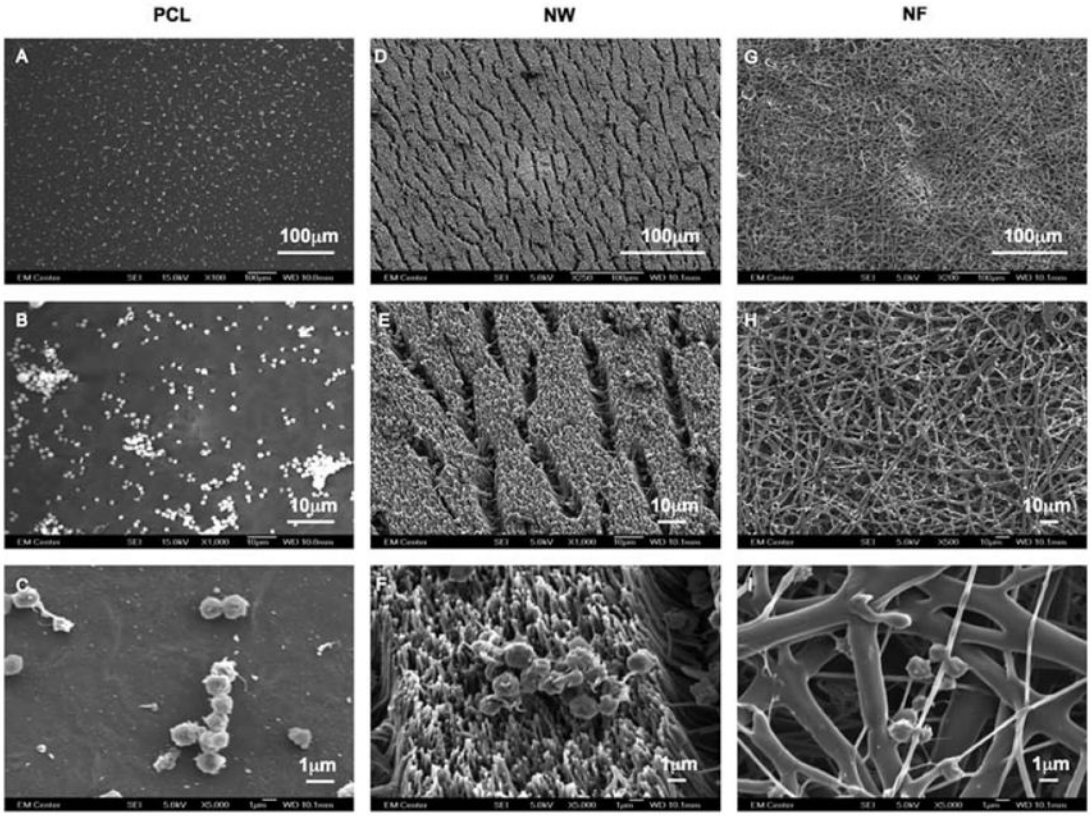

Figure 9.
Representative SEM images of adhered platelets on PCL (A, B and C), NW (D, E and F) and NF (G, H and I) surfaces.

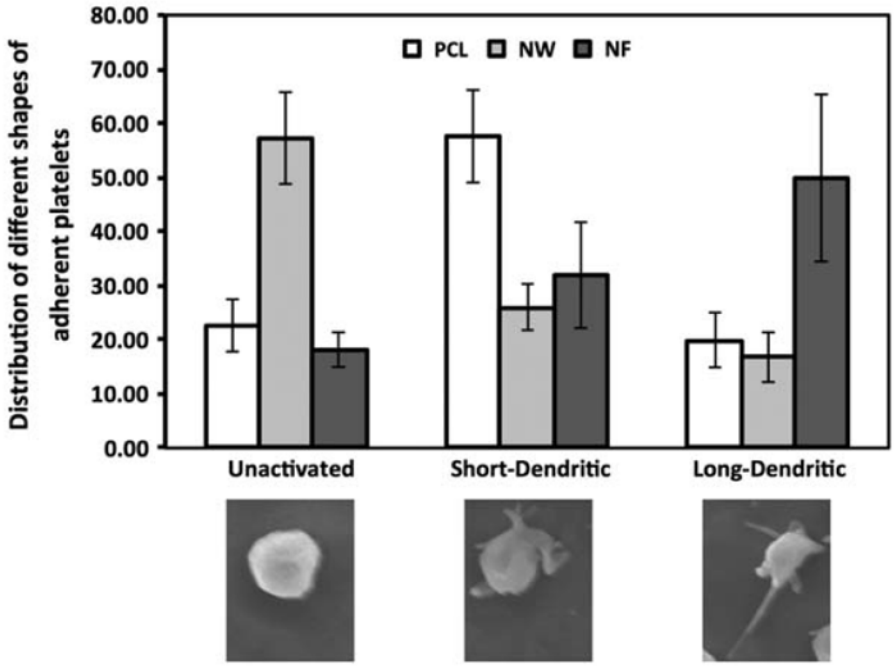

Figure 10.
Distribution of different shapes of adhered platelets on PCL, NW and NF surfaces. Representative morphology of platelets shown below the graph.

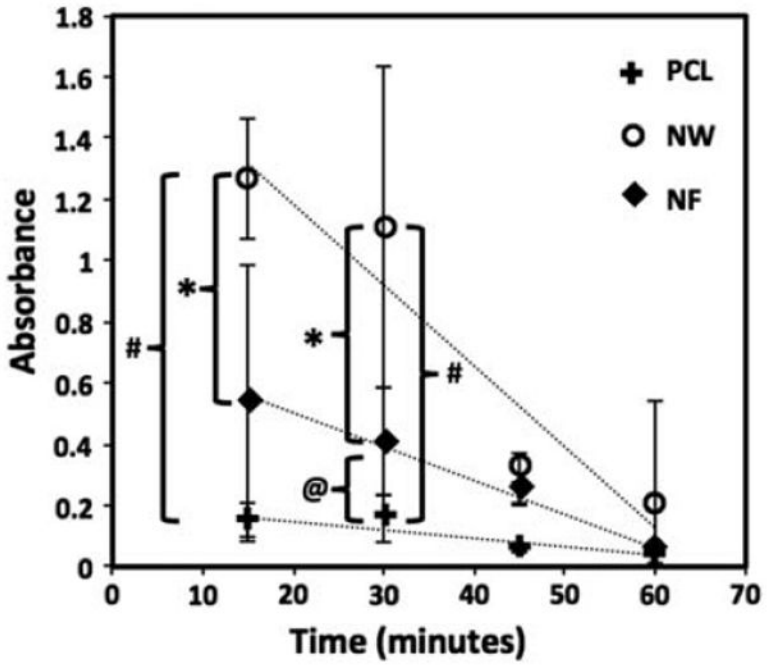

Figure 11.

Free hemoglobin concentration determined in terms of its absorbance on PCL, NW and NF surfaces for 60min of clotting time. Significant differences in free hemoglobin concentrations after 15mins on NW and NF surfaces, and NW and PCL surfaces (*, # → $p < 0.05$). Significant differences in few hemogblobin concentrations after 30mins on all surfaces (*, # and @ → $p < 0.05$).

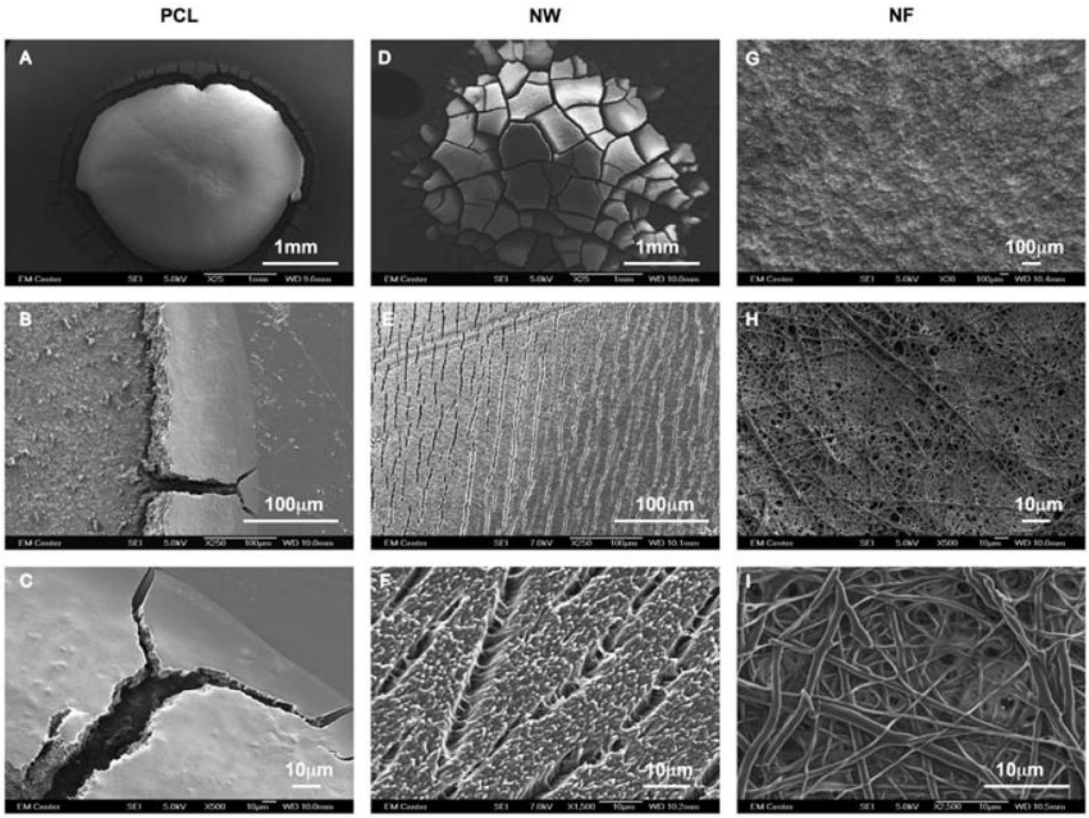

Figure 12.
Representative SEM images of whole blood clotted on PCL (A, B and C), NW (D, E and F) and NF (G, H and I) surfaces.

Table 1

Adsorption of key blood serum proteins ALB, FIB and IgG were investigated on PCL, NW and NF surfaces. The contribution of C-C, C-N and N-C=O peaks in the overall C1s peak are given as percentages.

		C-C	C-N	N-C=O
ALB	PCL	53.7	32.5	13.8
	NW	57.0	27.3	15.7
	NF	56.0	28.7	15.3
FIB	PCL	70.5	18.4	11.1
	NW	60.2	20.5	19.3
	NF	53.0	18.5	28.5
IgG	PCL	67.0	18.2	14.8
	NW	54.6	27.3	18.1
	NF	56.3	22.2	21.5